HAL
open science

Origin of Surface Reduction upon Water Adsorption on Oriented NiO Thin Films and Its Relation to Electrochemical Activity

Raphaël Poulain, Jochen Rohrer, Yannick Hermans, Christian Dietz, Joachim Brötz, Joris Proost, Marian Chatenet, Andreas Klein

To cite this version:

Raphaël Poulain, Jochen Rohrer, Yannick Hermans, Christian Dietz, Joachim Brötz, et al.. Origin of Surface Reduction upon Water Adsorption on Oriented NiO Thin Films and Its Relation to Electrochemical Activity. Journal of Physical Chemistry C, 2022, 126 (3), pp.1303-1315. 10.1021/acs.jpcc.1c07934 . hal-03736346

HAL Id: hal-03736346

https://hal.univ-grenoble-alpes.fr/hal-03736346

Submitted on 22 Jul 2022

HAL is a multi-disciplinary open access archive for the deposit and dissemination of scientific research documents, whether they are published or not. The documents may come from teaching and research institutions in France or abroad, or from public or private research centers.

L'archive ouverte pluridisciplinaire **HAL**, est destinée au dépôt et à la diffusion de documents scientifiques de niveau recherche, publiés ou non, émanant des établissements d'enseignement et de recherche français ou étrangers, des laboratoires publics ou privés.

Origin of surface reduction upon water adsorption on oriented NiO thin films and its relation to electrochemical activity

Raphaël Poulain[1,5], Jochen Rohrer[2], Yannick Hermans[1], Christian Dietz[3], Joachim Brötz[4], Joris Proost[5], Marian Chatenet[6], Andreas Klein[1,*]

[1] Technical University of Darmstadt, Institute of Materials Science, Electronic Structure of Materials, 64287 Darmstadt, Germany.
[2] Technical University of Darmstadt, Institute of Materials Science, Materials Modelling, 64287 Darmstadt, Germany.
[3] Technical University of Darmstadt, Institute of Materials Science, Physics of Surfaces, 64287 Darmstadt, Germany.
[4] Technical University of Darmstadt, Institute of Materials Science, Structural Research, 64287 Darmstadt, Germany.
[5] Université Catholique de Louvain, Materials and Process Engineering, 1348, Louvain-La-Neuve, Belgium.
[6] Université Grenoble Alpes, Grenoble INP, 38000 Grenoble, France.

Abstract

The interaction of water with oriented NiO films is studied using a combination of photoelectron spectroscopy with in-situ sample preparation and electrochemical measurements in the stability window of water. In contrast to NiO(100), room temperature water exposure induces a downward band bending on the (110)- and (111)-oriented films indicating a positive surface charge induced by a non-stoichiometric dissociative adsorption of water. Photoelectron spectroscopy suggests that the non-stoichiometric adsorption is related to the presence of adsorbed oxygen species. For the NiO(110) surface, these are identified using density functional theory calculations as bridging oxygen dimers. The preferential adsorption of protons, which requires interaction of two water molecules with the oxygen dimers, explains that water acts as an electron donor on many oxide surfaces. The different adsorption behaviour is consistent with the observation of a lower electrochemical activity of the (110)- and (111)-oriented surfaces towards hydrogen adsorption.

*corresponding author; email: aklein@esm.tu-darmstadt.de

1 Introduction

The efficiency of electrochemical water splitting, heterogeneous catalysis, gas sensor applications and inorganic/organic electronics depend strongly on the surface properties of the implemented inorganic materials, including the Fermi energy (E_{F}), the work function (ϕ) and the nature of the adsorbing sites.[1–4] These surface properties are expected to depend on the surface orientation, especially the work function.[5] The surface reactivity will be affected by the exposure of different amounts of cations and anions, which may provide Lewis acid and base sites for adsorption reactions. [6, 7]

The interaction of solid surfaces with water is of particular importance, as it is elemental to many chemical processes such as water splitting, purification, and corrosion. To understand these reactions, water adsorption studies are frequently carried out in ultrahigh vacuum, mostly at cryogenic temperatures where the amount of adsorbed water can be very accurately controlled down to fractions of a monolayer (see e.g. [8] and references therein). Water adsorption studies in vacuum can also be performed by exposing samples to water vapour at room temperature.[9–11] In the latter experiments, it has been observed that water has a strong reducing effect, as chemically reduced species and an upward shift of the Fermi energy are induced by water adsorption. A comparison of undoped with Co-doped $BiFeO_3$ suggests that the reduction has an electrochemical origin, that means it is the consequence of the raising Fermi energy.[11] It is therefore crucial to understand why water acts as an electron donor when adsorbed on oxide surfaces.

In this work, Nickel oxide (NiO) has been selected for studying the adsorption behaviour of water, as it can be prepared in-situ with different surface orientations. NiO crystallizes in the cubic rock salt structure. Its (100)- and (110)-oriented surfaces are non-polar (Tasker type I), while the (111)-orientated surface is polar (Tasker type III) with alternating Ni and O layers.[5, 12] The (100) facet has the lowest surface energy, for which the electronic structure is supposed to not differ substantially from bulk NiO.[13] The higher energy (110) and (111) surfaces could lead to geometrical (100) faceting.[14] The (111) surface can furthermore be stabilized by a p(2×2) octopolar reconstruction,[15] by chemical bonding with e.g. hydroxide [16, 17] or by the presence of nickel vacancies.[18]

Theoretical and experimental studies suggest that perfect (100)-oriented NiO surfaces are either not or only very little reactive towards oxygen species (O^-, O_2^-, O and O_2),[19] CO, H_2,[19] and water [20, 21] because the lowest excited states are far above the ground state making them chemically inaccessible for charge transfer.[22] However, NiO (100) surfaces become reactive if defects are introduced at the surface.[19, 20, 22, 23] Also, for single crystal NiO(100) surfaces, water can co-adsorb with oxygen near a defective site to form a stable hydroxide (OH^-).[21] Contrary to the (100) orientation, hydroxyl groups spontaneously form on the (111)-oriented surface when exposed to water,[20] where it has been reported that edges or corners between the (111) plane and (100)-reconstructed trigonal facets facilitate water dissociation.[24] Although the NiO

(110) orientation is the least practically studied surface orientation, theoretical studies highlighted that the NiO(110) orientation may be the most reactive facet towards methane dissociation.[23]

In this study, the surface properties of oriented nickel oxide thin films were studied using ultraviolet photoelectron spectroscopy (UPS) and X-ray photoelectron spectroscopy (XPS). The films were grown in-situ (see Fig. S1 in the supporting information for the experimental setup) by reactive direct current (DC) magnetron sputtering at high substrate temperature (400 °C) and various oxygen concentrations in the sputter gas on oriented platinum thin films. NiO thin film samples will be referred to by the orientation of the Pt substrate and by the oxygen concentration used during the respective thin film deposition. For instance, a NiO thin film prepared with an oxygen concentration of 10 % on MgO(100)/Pt becomes NiO(100)-10 %. The reactivity of the surfaces towards water was studied by exposing the samples to water vapour at room temperature inside the same vacuum system. To further distinguish the chemical surface properties, electrochemical measurements were performed in an oxygen-poor electrolyte (0.1 M NaOH) in the stability window of water. Details of the experimental techniques can be found in the supporting information.

2 Surface properties

XRD patterns of the NiO thin films (thickness $50 - 200$ nm) deposited on top of the oriented platinum thin films are displayed in Fig. 1(a). Details of the preparation and properties of oriented Pt substrates are reported in [25] and AFM images of Pt substrates are shown in Fig. S3 in the Supporting Information. Because of the low lattice mismatch between MgO and NiO (~ 1 %), it is not possible to differentiate the MgO peak from the NiO peak of the same orientation. However, the absence of other orientations confirms that fully (110)- and (111)-oriented NiO thin films have been obtained on MgO(110)/Pt and on α-sapphire(0001)/Pt, respectively, when the films were grown with an oxygen content of 20 % in the sputter gas. On the contrary, 10 % of oxygen during NiO deposition on MgO(100)/Pt substrates results in fully (100)-oriented NiO films. The dependence of the degree of orientation on the oxygen activity is in good agreement with literature.[26, 27]

AFM images of the NiO films in Fig. 1(b) reveal granular surfaces. According to a detailed analysis of the AFM images (see section S2 in the Supporting Information), the rms roughness of the films with unique orientation, (100)-10 %, (110)-20 %, and (111)-20 % are < 7 nm and the angles of the surface features are $< 45°$. Shadowing effects can be therefore be discarded, meaning that photoelectrons are collected from all parts of the surfaces. Moreover, the geometrical surface area is not more than 4 % higher than the projected surface area for the films with unique orientation. A stabilization of the polar (111) surface through pyramidal faceting as suggested in [14] is not evident from the AFM images.

X-ray photoelectron survey spectra (see Fig. S5 in the Supporting Infor-

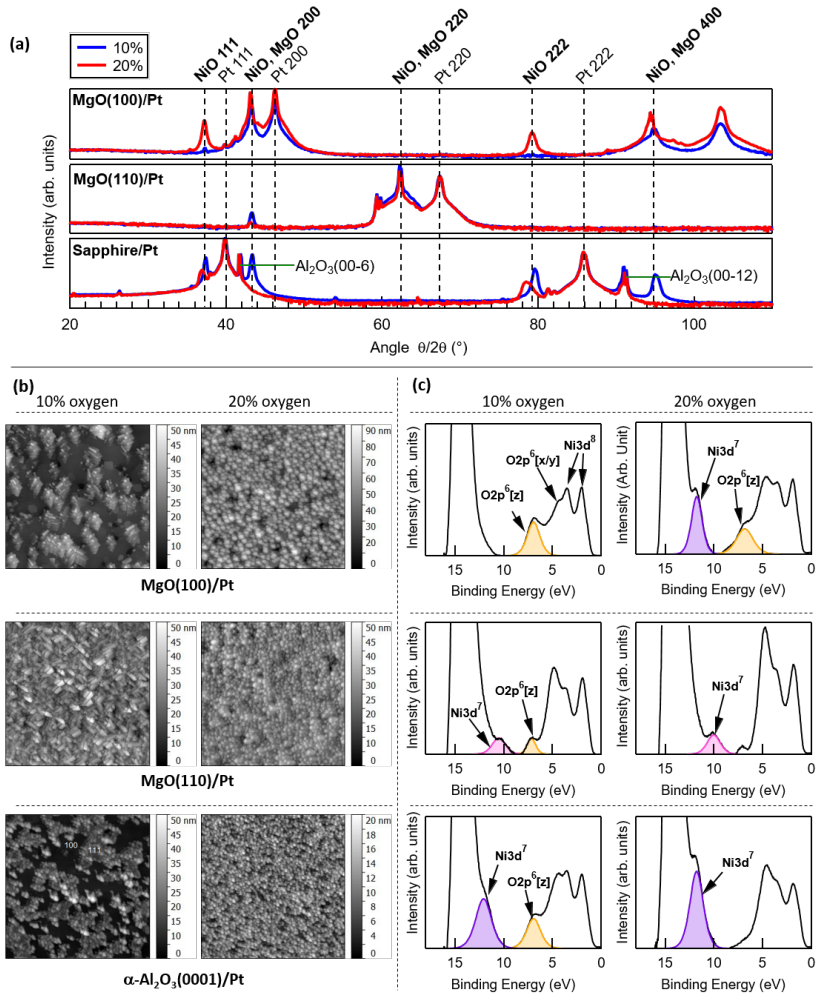

Figure 1: a) XRD scans of the NiO thin films deposited on MgO(100)/Pt, MgO(110)/Pt and α-Sapphire(0001)/Pt substrates at 400 °C and 10 % or 20 % of oxygen; b) AFM images ($3 \times 3\,\mu m^2$) measured on the same NiO thin films; c) surface electronic states measured by in-situ using UPS. Regarding the NiO thin films deposited on α-sapphire(0001)/Pt(111) at 10 %, the flat area associated to the (100) orientation is indicated by the label 100 while the grainy surface is associated to the (111) orientation indicated by the label 111.

mation) show no Pt signals, indicating absence of pinholes in NiO films, which might affect the electrochemical measurements. The same spectra further reveal that the as-deposited films show no carbon signals and also no other contaminations.

The UPS valence bands in Fig. 1(c) provide insights into the electronic structure of the NiO surfaces. The films with unique orientation display distinct surface electronic states. For instance, the UP spectrum of the (100)-oriented NiO film on MgO(100)/Pt with 10 % oxygen shows four features between 0 and 9 eV, in line with UP spectra obtained on (100) cleaved NiO single crystals.[21, 28] The two peaks in the lowest binding energy part can be associated to screened Ni $3d^8$ orbitals while the two features at higher binding energies can be attributed to final states associated to the O $2p^6$[x/y] and O $2p^6$[z] orbitals.[28] In the UP spectra of the (110)- and (111)-oriented NiO thin films, which were obtained on MgO(110)/Pt and on α-sapphire(0001)/Pt substrates with 20 % oxygen, respectively, only three features can be observed within the $0 - 9$ eV binding energy range. The absence of the O $2p^6$[z] state on dominantly (111)- and (110)-oriented surfaces is obvious. Similar observations are reported in literature for dominantly (111)-oriented NiO films.[24, 29] Emissions at 10 and at 11.7 eV can be observed for NiO films deposited on MgO(110)/Pt and on α-sapphire(0001)/Pt under 20 % of oxygen, respectively. This emission can be related to the Ni $3d^7$ state.[20, 30] UP-spectra of NiO films containing different orientations show the peaks specific for either orientation.

In summary, X-ray diffraction, atomic force microscopy and UPS confirm that the crystal and surface electronic structure of the prepared NiO thin films are highly (100)-oriented when deposited with 10 % O_2 on MgO(100)/Pt and highly (110)- and (111)-oriented when deposited with 20 % O_2 on MgO(110)/Pt and on α-sapphire(0001)/Pt, respectively.

Figure 2 displays XPS measurements obtained for oriented NiO thin films prepared at 400 °C after deposition, after water exposure in vacuum, and after the electrochemical cycling within the stability window of water. Additional survey, O $1s$ and C $1s$ spectra are shown in the Supporting Information. According to Taguchi *et al.*,[31] the Ni $2p$ region is the result of the contribution of the Ni $2p^5 3d^9 \underline{Z}$ (state in the $3d^9$ band), Ni $2p^5 3d^9 \underline{L}$ (state arising from the hybridization of the $3d^9$ band with the ligand) and the Ni $2p^5 3d^8$ orbitals. The states near the valence band maximum correspond to emissions from the Ni $3d^8 \underline{Z}$ state.

The main O $1s$ peak is found at ~ 530 eV, which accounts for the lattice O^{2-} species of NiO. For the freshly deposited samples, an additional weak photoelectron emission can be detected at a higher binding energy relative to the main peak (a detailed peak shape analysis of all recorded O $1s$ core level emissions is provided in the Supporting Information). This shoulder is stronger for deposition with higher oxygen concentration and for low deposition temperatures. Due to the dependence of the shoulder intensity on film orientation and oxygen content during film deposition and due to the different energy separation from the main line (1.8 eV as compared to 2.0 eV after water adsorption) we assign the weak high binding energy O $1s$ emission of the as-grown films to surface

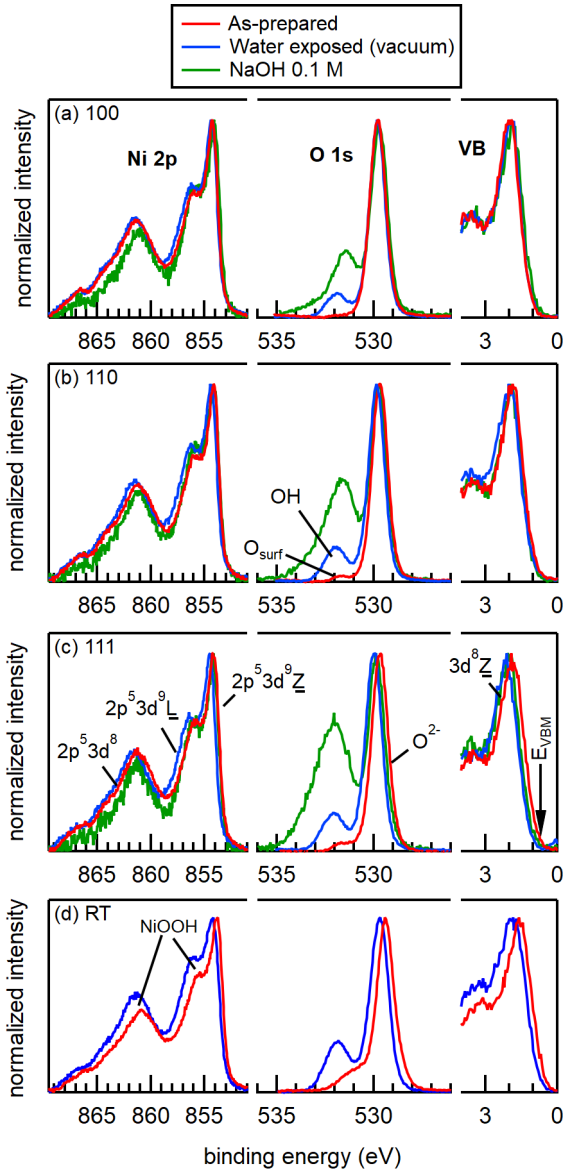

Figure 2: Ni $2p$, O $1s$ and the valence band (VB) XP-spectra of a) NiO(100)-10 %, b) NiO(110)-20 %, c) NiO(111)-20 %, and d) RT-NiO thin films. Intensities are normalized for better comparison. For the Ni $2p$ spectra difference traces are shown with respect to the as-prepared spectra. A comparison of the Ni $2p$ emission and detailed peak shape analysis of the O $1s$ emission is provided in the Supporting Information.

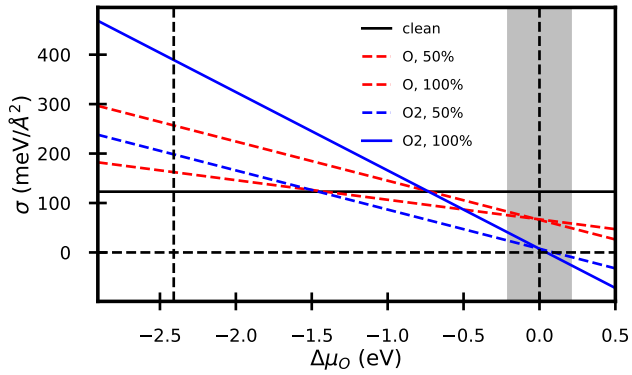

Figure 3: Surface-energy diagram of NiO(110) with various terminations/adsorbates. In the oxygen-poor limit the clean stoichiometric surface is favoured; in the oxygen-rich limit decoration with Ni-bridging O_2 dimers at 50% coverage is favoured. The gray-shaded area indicates the range of insecurity of the maximum oxygen chemical potential.

oxygen (O_{surf}) species, rather than to hydroxides.

In order to obtain more insights into the nature of the adsorbed oxygen species, we have performed density functional theory calculations of different surface terminations of symmetric (110)-oriented NiO slabs. In particular, we have considered bridging oxygen atoms and bridging oxygen dimers between two Ni atoms of neighboring Ni-O rows. The calculations revealed that adsorbed oxygen dimers stabilize the surface under oxidizing conditions (see Fig. 3). A schematic representation of the surface is given in Fig. 6. Details of the calculations and surface structures are given in the Supporting Information.

Surface reconstructions of the MgO(111) surface has been studied both experimentally and theoretically.[32–34] While the most stable surface reconstruction for most oxygen activities is the so-called "octupolar" reconstruction in which 3/4 of the atoms in the topmost layer and 1/4 of the atoms in the second layer are missing. This reconstruction can lead to either an O-rich or an Mg-rich termination but does not affect the oxidation state of oxygen and can therefore not explain the appearance of the surface oxygen emission at high binding energy. For high oxygen activity, different terminations of the (111) surface involving either oxygen trimers or dimers perpendicular to the surface become stable.[32]. Such species could explain the observation of the high binding energy shoulder in the O 1*s* spectrum of the as-deposited film. The stabilization of surface terminations calculated to be stable only at very high oxygen activity has also been observed for epitaxial In_2O_3 films, which were also grown with high oxygen content in the process gas.[35] As the NiO is isostructural to MgO with similar lattice constant, it is reasonable to assume that oxygen trimers and dimers are present at the NiO(111) surface under oxidizing preparation conditions.

3 Water exposure in vacuum

Water exposure was performed at room temperature by intermittently pulsing purified water with atomic layer deposition valves into a continuously pumped vacuum chamber connected to the XPS system (see the Supporting Information for details of the adsorption procedure and detailed analysis of XP spectra). The water pressure in the chamber is estimated to raise to $\sim 10\,\mathrm{Pa}$ during each $500\,\mathrm{ms}$ H_2O pulse and decrease in the consecutive pumping period.

Survey and C $1s$ XP spectra recorded after water exposure reveal only a very small carbon contamination (see Figs. S5 and S8(a) in the Supporting Information). After water exposure, the intensity of the photoelectron emission at the high binding energy side of the main O $1s$ peak increased for all studied surfaces. The binding energy difference to the main line is $\sim 2.0\,\mathrm{eV}$, $\sim 0.2\,\mathrm{eV}$ higher than before water exposure. The additional photoelectron emission after water exposure is associated to the formation of surface hydroxide species.[36, 37] In contrast to water adsorption at liquid nitrogen temperature [38–40] or to water exposure in an near-ambient pressure XPS setup,[41, 42] no ice or water layer is formed. This is evident from the absence of the typical H_2O related O $1s$ emission around $533\,\mathrm{eV}$. The hydroxide peak contributes 12–18 % to the total O $1s$ intensity, which corresponds to a $0.2 - 0.3\,\mathrm{nm}$ thick layer.

A detailed comparison of the Ni $2p$ spectra of the NiO thin films prepared at $400\,^{\circ}\mathrm{C}$ before and after water exposure is provided in section S3.3 in the Supporting Information. Water adsorption induces additional emissions in the $855 - 858\,\mathrm{eV}$ range, which overlaps with the Ni $2p^5 3d^9\underline{\mathrm{L}}$ feature. The Ni $2p$ region of the RT-NiO thin film is more affected by water exposure than the thin films produced at $400\,^{\circ}\mathrm{C}$, indicating a higher reactivity of the RT-NiO film. The additional feature induced by water exposure can be attributed to nickel hydroxide ($Ni(OH)_2$) and/or to nickel oxy-hydroxide (NiOOH).[43] According to electrochemical measurements performed at $1.1 - 1.3\,\mathrm{V}$ vs. RHE, the NiOOH phase spontaneously forms on RT-NiO thin films whereas $Ni(OH)_2$ is formed on the surfaces of NiO thin films prepared at high temperature (see section S4.4 in the Supporting Information). Therefore, the additional emissions in the Ni $2p$ spectra are associated to $Ni(OH)_2$ for the films prepared at $400\,^{\circ}\mathrm{C}$ but to NiOOH for films prepared at RT. The Ni $2p$ spectra of the $400\,^{\circ}\mathrm{C}$ films are very similar after water adsorption, which also agrees with the similar intensity of the hydroxide peak in the O $1s$ spectra. A slightly higher intensity of the Ni $2p$ spectrum of the (111)-oriented film in $855 - 858\,\mathrm{eV}$ range before water adsorption (see Fig. S6(g) in the Supporting Information) is likely attributed to the specific surface termination of the (111) surface.

Figure 4 displays the work functions, ϕ, obtained from the secondary electron cutoff of the UP valence band spectra as a function of the Fermi level position, $E_{\mathrm{F}} - E_{\mathrm{VB}}$. The valence band maxima from UPS and XPS and the core levels exhibit different binding energy shifts upon water adsorption. Three effects may contribute to the different shifts: i) the uncertainty in determining the valence band maximum in the XPS valence bands due to the absence of a sharp onset; ii) the contribution of adsorbed oxygen species to the electronic states near the

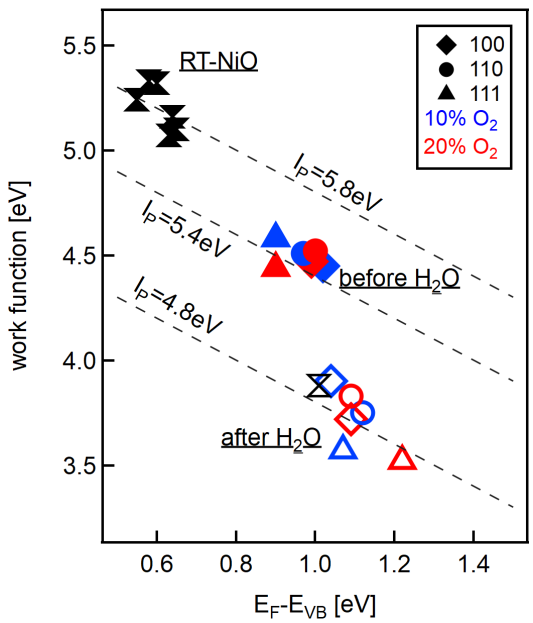

Figure 4: Work function vs. Fermi level position of NiO thin films after deposition (filled symbols) and after water exposure in vacuum (open symbols). The Fermi levels are derived from the binding energies of the O 1s core level as explained in section S3.7 in the supporting information. Diagonal solid lines represent constant ionization potentials I_{p}.

VBM,[44] which should contribute more in UPS due to the higher photoionization cross-section;[45] iii) the different surface sensitivity of the measurements in conjunction with the formation of a very narrow surface space charge region.[46] A detailed comparison of the binding energy shifts including the valence band maxima but also other binding energies extracted from the valence band and core level spectra is given in section S3.7 in the Supporting Information. From this analysis it is deduced that the most reliable quantity representing the surface Fermi level positions in Fig. 4 is the binding energy of the main O 1s line, which is extracted from the line profile analysis in section S3.4.

According to Fig. 4 the Fermi energies and ionization potentials ($I_{\mathrm{P}} = E_{\mathrm{vac}} - E_{\mathrm{VB}}$) samples grown at room temperature and at 400 °C are noticeably different. For the latter, the ionization potential decreases from 5.4 ± 0.5 eV to ~ 4.8 eV in the course of water adsorption. Given strongly different surface terminations and polarities, it is surprising that the ionization potential of the bare NiO surfaces does not depend on surface orientation and oxygen content during sample preparation. Such a behaviour, which is considered to be fortuitous, has also been observed for TiO_2,[9] CeO_2,[47], and SnO_2,[48] but not for In_2O_3.[35]

The change in Fermi energy upon water exposure is small for (100)-oriented NiO thin films, particularly for the film grown with 10 % oxygen. The largest increase of the Fermi energy upon water adsorption is observed for the (110)- and (111)-oriented films grown with 20 % oxygen. An increase of the Fermi energy indicates the formation of a positive surface charge, which is apparently not induced by water adsorption on NiO(100) but on the (110)- and (111)-oriented surfaces. The origin of this difference will be discussed in section 5.

4 Adsorption in an electrolyte

The NiO thin films studied in vacuum by in-situ XPS and UPS have been characterized in an oxygen-poor 0.1 M NaOH electrolyte by cyclic voltammetry (CV), chronoamperometry (CA) and electrochemical impedance spectroscopy (EIS) experiments. The experiments were constrained to the stability window of water ($0.1 - 1$ V vs. RHE) to avoid any drastic surface modification induced by the oxygen evolution reaction (OER, $E^{\mathrm{eq}} = 1.23$ V vs. RHE), the hydrogen evolution reaction (HER, $E^{\mathrm{eq}} = 0$ V vs. RHE) or to the nickel hydroxide to oxyhydroxide phase transformation ($E^{\mathrm{eq}} \approx 1.4$ V vs. RHE).[49, 50] According to the recently updated Pourbaix diagram for Ni derived compounds, NiO is stable in our experimental conditions and no surface reduction of the NiO electrode is expected.[51] Moreover, the analysis of the AFM images (see section S2 in the Supporting Information) indicate that the geometric surface area of the oriented films is not more than 4 % higher than the projected surface area. The electrochemical properties are therefore expected to be dominated by the nominal surface orientations.

Ni $2p$ spectra recorded after the electrochemical measurements are included in Fig. 2. The photoelectron emission in the range 854–860 eV does not increase when to compared to the spectra recorded after water adsorption (see section S3.3 in the Supporting Information). This indicates that the electrochemical experiments have no apparent effect on the hydroxide coverage of the surface. A substantial surface modification by carbonaceous species is also ruled out. The increase of the intensity of the high binding energy species in the O $1s$ emission is therefore not considered to be connected to changes of the NiO surface. As the samples have been extracted from the electrolyte and were exposed to air before XPS analysis, adsorption of species floating on the surface of the electrolyte or in the different environments, which do not directly interact with NiO species, are likely the origin of the high binding energy components. Such an assignment is also confirmed by the presence of different carbon species after electrochemical measurements. It is noted that the Ni $2p$ and O $1s$ spectra recorded after the electrochemical treatment in this work are very different from those obtained for comparable samples, which have been exposed to electrochemical measurements in the oxygen evolution regime.[49] In the latter case, the shoulder in the O $1s$ region and the region associated to nickel hydroxide in the Ni $2p$ region are dominating the spectra.

The results of the electrochemical experiments are displayed in Fig. 5. The

comparison of the CA experiments with the CV enables to differentiate currents associated to adsorption (and desorption) reactions from faradaic ones, which are continuous electrochemical reactions. As represented in Fig. 5(a), adsorption (and desorption) processes are indicated when the CA signal gradually levels off with time (right graph) whereas faradaic (continuous) electrochemical reactions are evidenced by a CA signal converging to the current value measured during the CV measurements (left graph).

The highly irreversible oxygen reduction (ORR, $E^{\mathrm{eq}} = 1.23\,\mathrm{V}$ vs RHE), is identified in the negative plateau in the $0.4 - 0.7\,\mathrm{V}$ vs. RHE. The ORR current is limited because of the nitrogen pre-conditioning of the solution. Indeed, for oxygen-saturated solution, the negative current in this intermediate potential range is substantially increased (See Fig. S12 in the Supporting Information). The faradaic reaction for the -NiO(100)-10 % sample in the very low potential region ($0.1 - 0.3\,\mathrm{V}$ vs. RHE) has been associated to the ORR as well, but as a result of a different kinetic mechanism. The ORR, which is characterized by a large polarization potential, can consist of multiple adsorption/desorption reactions and can produce numerous intermediate oxygen species in alkaline media.[52]

In addition, NiO surfaces could be subjected to reduction of a surface α-$Ni(OH)_2$ monolayer into metallic nickel between -0.1 and $+0.2\,\mathrm{V}$ vs. RHE on NiO_x surface [53, 54]:

$$\mathrm{Ni(OH)_2} + 2\,\mathrm{e}^- \rightarrow \mathrm{Ni}^0 + 2\ \mathrm{OH}^- \tag{1}$$

The surface reduction to Ni^0, as described by Eq. 1, should be accompanied by an obvious re-oxidation cathodic current for increasing potential sweep.[53, 54] Although unlikely, this option cannot be excluded. Eventually, in comparing the CV and the CA measurements in Fig. 5(b), adsorption reactions can be unveiled between $0.1 - 0.3\,\mathrm{V}$ vs. RHE and between $0.8 - 1.1\,\mathrm{V}$ vs. RHE. We assign these adsorption features to the hydrogen adsorption reaction and the hydroxide adsorption reaction, which are expected to dominate in the lower potential range and in the upper potential window, respectively.[55]

The adsorption reactions of hydrogen and hydroxide are also observed by EIS as a result of shortening of the bond length between these species and the electrode surface depending on the electrode potential. The stronger interaction of the adsorbates with the electrode surface results in the built-up of a charged double layer which is translated by an increase of the capacitive element measured by EIS.[6]

The electrochemical results display larger differences with the oxygen content during the film preparation than with the orientation of the substrates. For instance, in Fig. 5, it can be observed that, when the films are prepared with 10 % oxygen, the CV looks relatively inert in comparison to what is obtained with the samples prepared with 20 % oxygen. On the contrary, when the samples are prepared with 20 % of oxygen, the ORR, the hydrogen adsorption reaction, and the hydroxide adsorption reaction are enhanced. Concurrently, the EIS results show an obvious increase in adsorption in the potential range associated to the

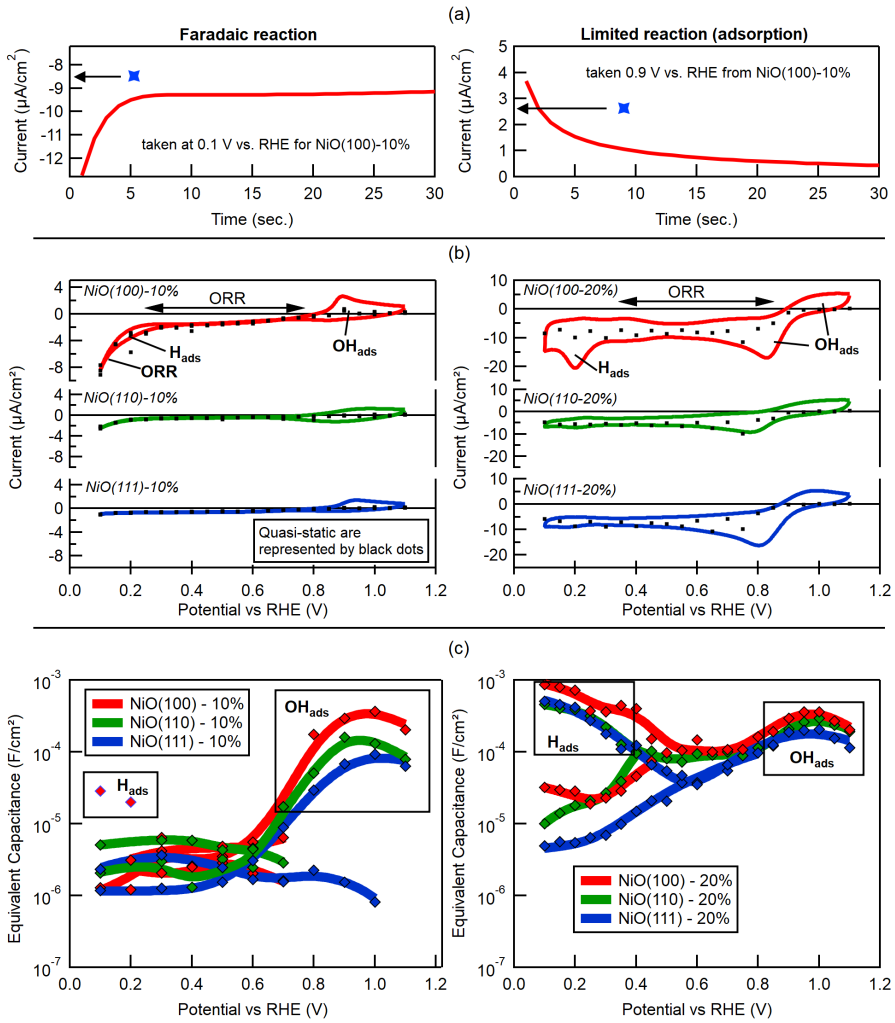

Figure 5: Electrochemical studies of oriented NiO thin films: (a) schematic time dependence of current in a chronoamperometry (CA) experiment. The values of the current during the cyclic voltammetry (CV) at the potential of the CA measurements are shown by the blue symbols. The left plot shows the typical CA convergence of a continuous reaction while the right plot shows CA decays relative to the CV values typical for an adsorption reaction. Electrochemical results regarding the CV and the CA measurements are shown in part (b) and the C_{CPE} measured by electrochemical impedance spectroscopy (EIS) in the stability window of water in (c).

hydrogen adsorption reaction for every samples prepared with 20 % of oxygen in comparison to the samples prepared with 10 % of oxygen. This increase in the adsorption activity of samples prepared in higher oxygen content is attributed to the presence of electronic (e.g. nickel vacancies) and structural (e.g. grain boundaries) defects that develop under such conditions. This is supported by the AFM images of the samples prepared with 20 % of oxygen, which indicate a smaller grain size. Preparation of films with a higher oxygen content may also result in a higher concentration of surface defects due to the bombardment with negatively charged oxygen ions generated in the plasma.[56] Water dissociation and chemical reactions are enhanced on defective surfaces in comparison to defect-free ones. [57, 58]

Interestingly, the electrochemical measurements indicate a higher activity of the (100) surface towards the hydrogen adsorption reaction. Indeed, in Fig. 5(c), the 10 %-NiO(100) oriented surface displays a remaining capacitive effect related to the adsorption of hydrogen while the corresponding CV displays a hysteresis in the low potential range in Fig. 5(b). Also, the CV obtained with the 20 %-NiO(100) surface displays a stronger adsorption feature related to the adsorption of protons (H^+) than on the dominantly (110)- and (111)-oriented films. The reason could be that the (110)- and (111)-oriented films provide less adsorption sites for the hydrogen adsorption reaction than the (100)-oriented surface.

5 Discussion

There is a general consensus from cryogenic-temperature adsorption studies that water spontaneously dissociates on the polar NiO(111) surfaces to form hydroxides [17, 20, 38] but dissociates on the non-polar NiO(100) surface only in the presence of defects or non-lattice oxygen. [19–23, 39, 40, 59] In contrast, the O $1s$, Ni $2p$ and UPS emissions of our room temperature water exposure experiments clearly indicate a comparable amount of hydroxide species on all studied surface orientations. This may, on the one hand, be related to a higher thermal energy at room temperature for overcoming activation barriers of reactions. On the other hand, the water vapour pressure in the experiments performed in this work is orders of magnitude higher than that used in cryogenic adsorption experiments. This increases the possibility for having simultaneously two water molecules available at the surface, which might be required to complete a reaction.

The products of water dissociation on the surfaces, H^+ and OH^-, are expected to adsorb on Lewis base (S_b) and acid (S_a) sites, respectively. It is generally accepted that Lewis acid and base sites on transition metal oxides have cationic and anionic character, which, in the case of NiO, are nickel and oxygen atoms. If both sites are available at neighboring locations on the surface, as it is the case for NiO(100), water adsorption can follow a stoichiometric dissociative adsorption reaction according to:

$$H_2O + S_b + S_a \rightarrow S_bH^+_{ads} + S_aOH^-_{ads} \tag{2}$$

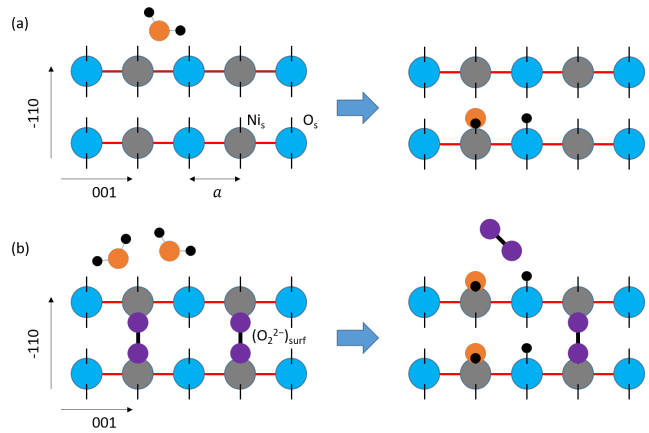

Figure 6: Schematic description of water adsorption on a bulk truncated NiO(110) surface following reaction 2 (a) and on a dimer-stabilized (110) surface according to reaction 3 (b). All images are top views on the NiO(110) surface. Red lines correspond to bulk Ni-O bonds. On the dimer-stabilized surface, 2 water molecules are required for dissociative adsorption, which results in the removal of an oxygen molecule. While the negative surface charge of the dimers is compensated by the hydroxides, the additional protons adsorbed on surface oxygen generate a net positively charged surface.

where S_a and S_b denote surface Lewis acid and base sites, respectively. As positive H^+ and negative OH^- species are equally adsorbed on the surface, no net surface charge is induced. Consequently, no change of the Fermi energy at the surface is expected, in agreement with the observation for the predominantly (100)-oriented surface. The adsorption behaviour described by Eq. 2 is also consistent with the electrochemical measurements of the (100)-oriented film, which shows activity for both hydrogen and hydroxide adsorption reactions. A stoichiometric adsorption reaction can also occur at the bulk-truncated NiO(110) surface, which is expected to be stable at low oxygen activity according to Fig. 3. The stoichiometric adsorption of water on NiO(110) is schematically illustrated in Fig. 6(a).

In contrast to the (100) surface, the increase of the Fermi energy at the (110)- and (111)-oriented surfaces induced by water exposure indicates the formation of a positive surface charge. It is suggested that this difference is related to the presence of the surface oxygen species. For example, the formation of a positive surface charge on the dimer-stabilized NiO(110) surface upon water exposure is suggested to proceed as:

$$2\mathrm{Ni_s} + (\mathrm{O_2^{2-}})_{\mathrm{ads}} + 2\mathrm{O_s} + 2\mathrm{H_2O} \rightarrow 2\mathrm{Ni_sOH^-_{ads}} + 2\mathrm{O_sH^+_{ads}} + \mathrm{O_2} + 2\mathrm{e^-} \qquad (3)$$

where Ni_s and O_s are Ni and O lattice atoms at the surface. The adsorption results in a release of an oxygen molecule and of two electrons. The negative

charge of the dimer is replaced by an identical charge of the two hydroxide species. In addition, the two adsorbed protons generate a net positive surface charge and the generation of 2 electrons. This is considered to be the origin of the raising Fermi energy upon water adsorption observed in XPS and UPS.

Water adsorption is typically discussed to occur stoichiometrically and may result in various bonding geometries depending on surface orientation.[60–64] However, using the same adsorption setup as in the present study, an increase of the Fermi energy upon room temperature water exposure has been observed for several oxides including anatase TiO_2,[9] $BiFeO_3$,[11] $BiVO_4$,[10] and $CuFeO_2$,[65] indicating that the effect is quite general. For anatase TiO_2, Kashiwaya et al. have also found that the changes of the Fermi energy are very similar for different surface preparation conditions on for both single crystalline (101) and (001) surfaces as well as for polycrystalline thin films.[9] The upward shift of the Fermi energy is a notable phenomenon as it can induce an electrochemical reduction of the material.[10, 11] The shifts are unexpected since the HOMO of water lies about 7 eV below the conduction band minimum of the metal oxides, which should exclude electron injection. The suggested non-stoichiometric dissociative adsorption of H_2O, which is associated with the removal of adsorbed oxygen dimers or related surface species, provides a reasonable explanation for the shift of the Fermi energy.

An important aspect of the adsorption reaction 3 is that two water molecules are required. The reaction can therefore only take place at sufficiently high water vapour pressure. Therefore, an adsorption experiment at room temperature in a high water vapour pressure can lead to a different result as an experiment carried out at cryogenic temperatures at low vapour pressure. As estimated above, a water pressure of $\sim 10\,\mathrm{Pa}$ is reached in the present experiment, while low temperature water adsorption studies are typically carried out using leak valve dosing at water pressures of $\sim 10^{-6}\,\mathrm{Pa}$. In addition to the lower thermal activation at cryogenic temperatures, water may adsorb only molecularly on oxidized surfaces at low temperature due to the lower availability of water species. The requirement of a high vapour pressure of water to remove surface oxygen dimers will also protect the dimer-stabilized surface against hydroxilation from the water species in the residual gas of the vacuum system.

The electrochemical measurements suggest a lower activity of the (110) and (111) surfaces towards the hydrogen adsorption reaction. This can be interpreted by inactive or a less Lewis base sites, which are generally located on oxygen atoms. Eventually, we assume that the Lewis base sites, present in the form of surface oxygen, are reacting and eliminated from the surface during the adsorption reaction together with the oxygen from water molecules. The result is a non-stoichiometric dissociative adsorption of H_2O, the formation of a positively charged surface and the injection of electrons into the NiO substrate. Therefore, the proposed reaction scheme for the (110)-oriented surface explains both the change of the Fermi energy upon water exposure and the lower electrochemical activities towards the hydrogen adsorption reaction.

6 Summary and Conclusion

Surface properties of NiO thin films grown on oriented platinum thin films at 400 °C by magnetron sputtering have been studied using photoelectron spectroscopy and electrochemical measurements. Highly oriented NiO thin films can be obtained on MgO(100)/Pt, MgO(110)/Pt, and α-Sapphire(0001)/Pt by adjusting the oxygen content in the process gas. The surface electronic properties of the films exhibit unique features of the particular surface orientations. The crystalline NiO films exhibit work functions of ~ 4.5 eV and ionization potentials of ~ 5.4 eV. These values are ~ 0.4 eV smaller than those obtained for films deposited at room temperature. Except for the (100)-oriented film, the samples exhibit a high binding energy O $1s$ emission, which is ascribed to adsorbed oxygen species. Using DFT calculations, we have identified these species for the NiO(110) surface as bridging oxygen dimers. By analogy to DFT calculations on isostructural MgO(111) surfaces, oxygen trimers and dimers are suggested to be present on the NiO(111) surface.

Adsorption of water by exposure of the samples to a high water vapour pressure at room temperature exposure in a vacuum system occurs dissociatively for all surface orientations. The ionization potential is lowered by ~ 0.5 eV. In addition, all samples exhibit hydroxide emissions in the O $1s$ and the Ni $2p$ core levels. A substantial upward shift of the Fermi energy upon water adsorption is observed only on the (110)- and (111)-oriented films but not on NiO(100). Combining these observations, it is proposed that the change of the Fermi energy is caused by a non-stoichiometric dissociative adsorption of water, which leads to a removal of O_2 from the surface, a preferential adsorption of protons, and the injection of electrons. The bare NiO(100) surface, which is the thermodynamically most stable one and which does not require substantial surface reconstruction, exposes an equal number of adsorption sites for OH^- and H^+ resulting in no net surface charge after water dissociation.

The vacuum adsorption studies can be put in perspective with the electrochemical measurements, which reveal that hydroxide adsorption sites are present on all surfaces but only (100)-oriented films provide a higher activity towards hydrogen adsorption.

This work was funded by the European Union's Horizon 2020 research and innovation programme under the Marie Sklodowska-Curie grant agreement No. 641640 (EJD-ITN project FunMAT). JR acknowledges computational resources provided by the Lichtenberg high-performance computer of the TU Darmstadt.

References

[1] F. Mirabella, E. Zaki, F. Ivars-Barceló, X. Li, J. Paier, J. Sauer, S. Shaikhutdinov, and H.-J. Freund, Angew. Chem. Int. Ed. **57**, 1409 (2018).

[2] H. Fukagawa, M. Hasegawa, K. Morii, K. Suzuki, T. Sasaki, and T. Shimizu, Adv. Mater. **31**, 1904201 (2019).

[3] M. T. Greiner, M. G. Helander, W.-M. Tang, Z.-B. Wang, Z.-B. Wang, J. Qiu, and Z.-H. Lu, Nat. Mater. **11**, 76 (2012).

[4] M. T. Greiner, L. Chai, M. G. Helander, W. M. Tang, and Z. H. Lu, Adv. Funct. Mater. **22**, 4557 (2012).

[5] J. Goniakowski, F. Finocchi, and C. Noguera, Rep. Prog. Phys **71** (2008).

[6] S. Morrison, Electrochemistry at semiconductor and oxidized metal electrodes (Plenum Press, 1980).

[7] C. Jia, W. Fan, F. Yang, X. Zhao, H. Sun, P. Li, and L. Liu, Langmuir **29**, 7025 (2013).

[8] U. Diebold, Surf. Sci. Rep. **48**, 53 (2003).

[9] S. Kashiwaya, J. Morasch, V. Streibel, T. Toupance, W. Jaegermann, and A. Klein, Surfaces **1**, 73 (2018).

[10] Y. Hermans, S. Murcia-López, A. Klein, and W. Jaegermann, ACS Energy Lett. **4**, 2522 (2019).

[11] N. S. Bein, P. Machado, M. Coll, F. Chen, M. Makarovic, T. Rojac, and A. Klein, J. Phys. Chem. Lett. **10**, 7071 (2019).

[12] P. W. Tasker, J. Phys. C. **12**, 4977 (1979).

[13] M. R. Castell, S. L. Dudarev, P. L. Wincott, N. G. Condon, C. Muggelberg, G. Thornton, D. Nguyen Manh, A. P. Sutton, and G. A. D. Briggs, Surf. Rev. Lett. **04**, 1003 (1997).

[14] B. Warot, E. Snoeck, J. C. Ousset, M. J. Casanove, S. Dubourg, and J. F. Bobo, Appl. Surf. Sci. **188**, 151 (2002).

[15] A. Barbier, C. Mocuta, H. Kuhlenbeck, K. F. Peters, B. Richter, and G. Renaud, Phys. Rev. Lett. **84**, 2897 (2000).

[16] M. A. Langell and M. H. Nassir, J. Phys. Chem. **99**, 4162 (1995).

[17] N. Kitakatsu, V. Maurice, C. Hinnen, and P. Marcus, Surf. Sci. **407**, 36 (1998).

[18] P. M. Oliver, S. C. Parker, and W. C. Mackrodt, Model. Simul. Mater. Sci. Eng **1**, 755 (1993).

[19] J. M. Blaisdell and A. B. Kunz, Phys. Rev. B **29**, 988 (1984).

[20] D. Cappus, C. Xu, D. Ehrlich, B. Dillmann, C. A. Ventrice, K. Alshamery, H. Kuhlenbeck, and H. J. Freund, Chem. Phys. **177**, 533 (1993).

[21] J. M. McKay and V. E. Henrich, Phys. Rev. B **32**, 6764 (1985).

[22] G. T. Surratt and A. B. Kunz, Phys. Rev. Lett. **40**, 347 (1978).

[23] J. J. Varghese and S. H. Mushrif, J. Phys. Chem. C **121**, 17969 (2017).

[24] L. Liu, S. Wang, S. Liu, Q. Guo, and J. Guo, Surf. Sci. **667**, 8 (2018).

[25] K. Rachut, T. J. M. Bayer, J. O. Wolff, B. Kmet, A. Benčan, and A. Klein, phys. status solidi (b) **256**, 1900148 (2019).

[26] W. L. Jang, Y. M. Lu, W. S. Hwang, T. L. Hsiung, and H. P. Wang, Surf. Coat. Tech. **202**, 5444 (2008).

[27] H. W. Ryu, G. P. Choi, G. J. Hong, and J. S. Park, Jpn J. Appl. Phys. **43**, 5524 (2004).

[28] H. Kuhlenbeck, G. Odörfer, R. Jaeger, G. Illing, M. Menges, T. Mull, H. J. Freund, M. Pöhlchen, V. Staemmler, S. Witzel, et al., Phys. Rev. B **43**, 1969 (1991).

[29] S. Wang, S. M. Liu, J. D. Guo, K. H. Wu, and Q. L. Guo, Surf. Sci. **606**, 378 (2012).

[30] S. Hüfner, Adv. Physic **43**, 183 (1994).

[31] M. Taguchi, M. Matsunami, Y. Ishida, R. Eguchi, A. Chainani, Y. Takata, M. Yabashi, K. Tamasaku, Y. Nishino, T. Ishikawa, et al., Phys. Rev. Lett. **100**, 206401 (2008).

[32] Q. Zhu, L. Li, A. R. Oganov, and P. B. Allen, Phys. Rev. B **87**, 195317 (2013).

[33] W.-B. Zhang and B.-Y. Tang, J. Phys. Chem. C **112**, 3327 (2008).

[34] R. Plass, K. Egan, C. Collazo-Davila, D. Grozea, E. Landree, L. D. Marks, and M. Gajdardziska-Josifovska, Phys. Rev. Lett. **81**, 4891 (1998).

[35] M. Hohmann, P. Ágoston, A. Wachau, T. J. M. Bayer, J. Brötz, K. Albe, and A. Klein, J. Condens. Matter Phys. **23**, 334203 (2011).

[36] M. Fingerle, S. Tengeler, W. Calvet, T. Mayer, and W. Jaegermann, J. Electrochem. Soc. **165**, H3148 (2018).

[37] J.-C. Dupin, D. Gonbeau, P. Vinatier, and A. Levasseur, Phys. Chem. Chem. Phys. **2**, 1319 (2000).

[38] M. Schulze, R. Reissner, M. Lorenz, U. Radke, and W. Schnurnberger, Electrochim. Acta **44**, 3969 (1999).

[39] R. Reissner and M. Schulze, Surf. Sci. **454-456**, 183 (2000).

[40] M. Schulze and R. Reissner, Surf. Sci. **482-485**, 285 (2001).

[41] J. T. Newberg, D. E. Starr, S. Yamamoto, S. Kaya, T. Kendelewicz, E. R. Mysak, S. Porsgaard, M. B. Salmeron, G. E. Brown, A. Nilsson, et al., J. Phys. Chem. C **115**, 12864 (2011).

[42] G. Ketteler, S. Yamamoto, H. Bluhm, K. Andersson, D. E. Starr, D. F. Ogletree, H. Ogasawara, A. Nilsson, and M. Salmeron, J. Phys. Chem. C **111**, 8278 (2007).

[43] M. C. Biesinger, B. P. Payne, L. W. M. Lau, A. Gerson, and R. S. C. Smart, Surf. Interface Anal. **41**, 324 (2009).

[44] P. Ágoston, P. Erhart, A. Klein, and K. Albe, J. Phys.: Cond. Matter **21**, 455801 (2009).

[45] J. J. Yeh and I. Lindau, Atomic Data and Nuclear Data Tables **32**, 1 (1985).

[46] A. F. Zurhelle, X. Tong, A. Klein, D. S. Mebane, and R. A. D. Souza, Angew. Chem. Int. Ed. **56**, 14516 (2017).

[47] H. Wardenga and A. Klein, Appl. Surf. Sci. **377**, 1 (2016).

[48] K. Rachut, C. Körber, J. Brötz, and A. Klein, phys. stat. sol. (a) **211**, 1997 (2014).

[49] R. Poulain, A. Klein, and J. Proost, J. Phys. Chem. C **122**, 22252 (2018).

[50] M. Alsabet, M. Grden, and G. Jerkiewicz, Electrocatalysis **5**, 136 (2014).

[51] L.-F. Huang, M. J. Hutchison, R. J. Santucci, J. R. Scully, and J. M. Rondinelli, J. Phys. Chem. C **121**, 9782 (2017).

[52] X. Ge, A. Sumboja, D. Wuu, T. An, B. Li, F. W. T. Goh, T. S. A. Hor, Y. Zong, and Z. Liu, ACS Catal. **5**, 4643 (2015).

[53] A. G. Oshchepkov, A. Bonnefont, and E. R. Savinova, Electrocatalysis **11**, 133 (2020).

[54] M. Grdeń, M. Alsabet, and G. Jerkiewicz, ACS Appl. Mater. Interfaces **4**, 3012 (2012).

[55] A. Bagger, R. M. Arán-Ais, J. Halldin Stenlid, E. Campos dos Santos, L. Arnarson, K. Degn Jensen, M. Escudero-Escribano, B. Roldan Cuenya, and J. Rossmeisl, ChemPhysChem **20**, 3096 (2019).

[56] K. Ellmer and T. Welzel, J. Mater. Res. **27**, 765 (2012).

[57] R. H. Head, C. Gattinoni, L. Trotochaud, Y. Yu, O. Karslıoğlu, S. Pletincx, B. Eichhorn, and H. Bluhm, J. Phys. Chem. C **123**, 16836 (2019).

[58] J. Liu, Z. Wei, and W. Shangguan, ChemCatChem **11**, 6177 (2019).

[59] A. Zangwill, Physics at Surfaces (Cambridge University Press, 1988).

[60] M. A. Henderson, Surf. Sci. Rep. **46**, 1 (2002).

[61] D. R. Mullins, P. M. Albrecht, T.-L. Chen, F. C. Calaza, M. D. Biegalski, H. M. Christen, and S. H. Overbury, J. Phys. Chem. C **116**, 19419 (2012).

[62] R. R. Rao, M. J. Kolb, J. Hwang, A. F. Pedersen, A. Mehta, H. You, K. A. Stoerzinger, Z. Feng, H. Zhou, H. Bluhm, et al., J. Phys. Chem. C **122**, 17802 (2018).

[63] J. Heras-Domingo, M. Sodupe, and X. Solans-Monfort, J. Phys. Chem. C **123**, 7786 (2019).

[64] U. Diebold, J. Chem. Phys. **147**, 040901 (2017).

[65] Y. Hermans, A. Klein, H. P. Sarker, M. N. Huda, H. Junge, T. Toupance, and W. Jaegermann, Adv. Funct. Mater. **30**, 1910432 (2020).